Non-linear light scattering in polar oxides at the example of strontium-barium-niobate

M. Imlau
Fachbereich Physik, Universität Osnabrück, Barbarastr. 7, D-49069 Osnabrück, Germany

Th. Woike
Institut für Mineralogie und Geochemie, Universität zu Köln, Zülpicherstr. 49b, D-50674 Köln, Germany

M. Fally, M. Ellaban and R. A. Rupp
Institut für Experimentalphysik, Universität Wien, Boltzmanngasse 4, A-1090 Wien, Austria

M. Goulkov
Institute of Physics, National Academy of Sciences of Ukraine, Science Ave 46, 03650 Kiev, Ukraine

Illumination of photorefractive crystals leads to the build-up of an extremely pronounced light scattering beside the directly transmitted beam. The spatial intensity distribution and the pattern formation are shown to result from multi-wave interactions of initially scattered waves with the pump wave, whereby crystal symmetry, nature and properties of the photorefractive effect and seed scattering centers play an important role. In the most common explanation non-linear light scattering results from the interference of scattered light with the pump beam, thus resulting in a complex light interference pattern, which is transferred into a complex modulation of the refractive index. A hologram of the seed scattering is recorded, showing properties comparable to volume holographic phase gratings: the scattering phenomenon is bound to the existence of the Bragg-condition and therefore vanishes, when wavelength or read-out angle of the pump beam configuration are violated. An essential point for the build-up of a pronounced light scattering distribution is the existence of a light amplification process, which occurs e.g. in materials with a non-local photorefractive response via beam-coupling. Non-linear light scattering is observed in a multitude of photorefractive media, and is commonly reported as a serious drawback in the frame of applications, since it reduces the signal-to-noise ratio. This review summarizes the most important features of non-linear light scattering, describes the different kinds of multi-wave interactions and amplification processes and gives an insight into the most recent progress in the understanding of this phenomenon. New methods for material characterization are presented based on the analysis of non-linear light scattering at the example of the photorefractive polar oxide strontium-barium-niobate.

PACS numbers:

I. INTRODUCTION

The effect of non-linear light scattering has first been recognized in 1966 by Ashkin et al., who observed the temporal evolution of a wide-angle scattering distribution when a crystal of lithium-niobat was exposed to coherent laser light [1]. It was the starting point of the photorefractive effect in polar oxidic crystals, which is attributed to the electro-optic effect and which was utilized for a multitude of applications in the field of non-linear optics, such as the recording of elementary holographic gratings [2, 3]. In contrast, the effect of non-linear light scattering itself is commonly reported as a serious drawback in the field of applications, since a dynamical background scattering noise can rather be suppressed and, therefore, it reduces the signal-to-noise ratio, dramatically [4].

Non-linear light scattering is observed in a multitude of photorefractive materials: illumination with an unexpanded laser beam leads to the build-up of scattered light into a wide apex angle around the directly transmitted laser beam. Hereby, the pump beam intensity is decreased, which can be as effective as 99% with respect to the incoming laser light power, i.e. the incoming pump beam is nearly completely scattered. Two characteristic properties of this scattering process have to be emphasized: a) the build-up of the scattered light is observed within a timescale of several minutes, and, thereby comparable to the temporal behavior known from the recording of holographic gratings in such materials and b) the scattering process decreases strongly, if wavelength or angle of the read-out beam are changed with respect to the pump-beam configuration. This property is comparable to the behavior of volume holographic gratings, which are bound to the Bragg-condition, and is the reason, why the effect is commonly called *holographic light scattering* [5]. Further designations are photoinduced [6], light-induced light scattering [7] or stimulated photorefractive scattering [8]. It is called beam fanning [9] or occasionally random beam fanning [10, 11] if the scattering effect is characterized by a significant change of the intensity profile of the directly transmitted pump beam. Optical damage additionally describes phenomena accompanied by focussing or de-focussing processes [12].

Non-linear light scattering exhibits with coherent light,

only [13]. The elementary process can be understood in the frame of the interference of the pump beam with initial scattered waves: If a coherent laser beam propagates through a photorefractive crystal it is scattered at inhomogeneities, such as striations, defects or imperfections. Scattered waves exhibit, which interfere with the pump waves, resulting in a complex light interference pattern, which is transferred into a refractive index modulation via the photorefractive effect. This means, that a phase hologram of the initially scattered waves is recorded, which allows to reconstruct the scattered waves in intensity and spatial distribution if illuminated. Bright light scattering is observed, if there is an interaction between reconstructed and initial scattered waves, which results in an enhancement of the intensity. In this case non-linear light scattering can be understood in the frame of four-waves interaction phenomena: two waves record a "parasitic" hologram, at which diffraction of a third wave results into a fourth one. The common process of non-linear light scattering refers to a pair of recording waves (1 and 2), which is identical to the read-out wave pair (3 and 4) and leads to the above mentioned wide-angle scattering phenomena. Other processes, which include phase matching conditions between the four waves, result in spatially limited scattering pattern, e.g. scattering waves propagating on the rim of narrow cones (conical scattering [14]). Parametric scattering is observed if wave mixing of the two wave pairs occurs [15].

Obviously, there are two necessary conditions to obtain non-linear light scattering: a) scattering sources, such as crystal defects, surface scratches, refractive-index inhomogeneities [16], which are responsible for the initially scattered waves and b) an amplification process that leads to an enhancement of these waves. Holographic amplification for example is a result from two-beam coupling in materials with a non-local photorefractive response, i.e. materials, where the recorded refractive index modulation is phase-shifted with respect to the incoming light interference pattern [17, 18]. In this case non-linear light scattering compulsorily mirrors the specific nature of the photorefractive effect, i.e. the charge transport mechanism.

Taking the necessary assumptions into account, non-linear light scattering occurs in all photorefractive materials, i.e. materials, where the refractive index can be changed by light-illumination. Differences between scattering patterns are due to different interactions schemes between pump- and scattered waves. Two-wave [19–24], three-wave [21, 25–27], and four wave phenomena [28, 29] are reported. The result is a variety of steady-state pattern observed in different photorefractive materials ranging from two rings in photopolymers [30–32], "dots", ring patterns, or lobes of scattered light in $LiNbO_3$ [1, 6, 19, 21, 26, 33–38], a more complex lobe structure, "dots", rings and lines in $BaTiO_3$ [21, 26, 27, 39–47], diffracted lobes in $LiTaO_3$ [25, 29, 48], to a homogeneous isotropic scattering distribution [49] and a sharp scattering ring caused by flip scattering [50] in sodiumnitroprusside.

In this review we present the recent progress in investigations and understanding of the phenomenon of non-linear light scattering. The results are an extension of our previously published review [51], which is summarized in its essential fundamental parts. Progress is demonstrated at the example of strontium-barium-niobate, which is an excellent representative for materials with a nonlocal photorefractive response caused by diffusion transport mechanisms [52].

II. COMMON EXPLANATION FOR NON-LINEAR LIGHT SCATTERING

Non-linear light scattering is commonly explained by the recording of parasitic holographic phase gratings via small-signal amplification [19, 21, 53]. Coherent light is scattered at the entrance face of the photorefractive material due to e.g. scratches and at inhomogeneities within the crystal volume, e.g. due to imperfections, striations or defects (see Fig. 1a). The scattered light is called initial scattering or seed scattering. Initially scattered waves and the incoming pump wave are coherent to each other, so that a complex light pattern occurs by interference, which is transferred in photorefractive materials into a complex refractive index modulation (1b). A hologram of the initially scattered waves is recorded, which can be regarded as an overlap of a multitude of elementary holographic parasitic gratings, each recorded by a pair of one scattered wave with the pump wave.

Simultaneously to the recording mechanism the already recorded parasitic gratings are read-out by the pump beam, i.e. the pump beam is diffracted (1c). Reconstructed and initially scattered waves may differ in intensity and phase depending on the recording mechanism. In the case of constructive interference the extremely small intensity of the initially scattered light will increase. The essential phase shift can be observed in photorefractive materials with a non-local photorefractive effect. Here, the phase of the reconstructed scattered wave is shifted by $\pi/2$ with respect to the phase of the scattered wave, which general holds for diffraction processes at phase gratings. An additional phase-shift of $\pi/2$ results from the non-local photorefractive response, i.e. the phase grating is shifted by $\Lambda/4$ with respect to the incoming light interference pattern (Λ: spatial period of the grating). As a result the reconstructed scattered wave will be π-shifted in its phase and constructive interference with the initially scattered wave occurs. The scattering intensity increases and the light interference pattern and refractive index modulation, respectively, are enhanced. In the following diffraction and interference processes lead to a feed-back mechanism, which finally amplifies the scattered light to extremely large intensities. This effect is commonly known as beam-coupling and describes the energy exchange between a small signal and a strong pump beam. At the same time, it is

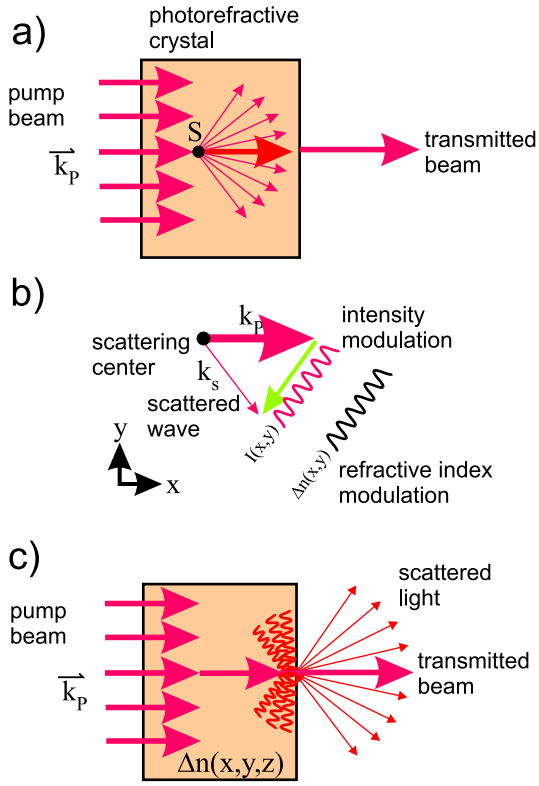

FIG. 1: a) The incoming pump beam $\mathbf{k_P}$ is scattered at the scattering center S. b) The scattered wave $\mathbf{k_s}$ interferes with the propagating pump beam. A sinusoidal light interference pattern $I(z)$ occurs, which is transferred into a refractive-index modulation $\Delta n(z)$ via the photorefractive effect. c) The pump beam is diffracted at the recorded refractive index modulation. If scattered and diffracted waves interfere constructively, the scattered light is amplified and can be observed beside the directly transmitted laser beam.

obvious, that beam coupling leads in addition to a depletion of the pump beam. Although the efficiency is extremely small regarding only the interaction of one scattered wave with the pump beam, pump beam depletion is an extremely pronounced effect, when multi-wave beam-coupling is taken into account. In some cases it results in the disappearance of nearly the complete intensity of the directly transmitted laser beam. Both processes of amplification and depletion, respectively, can be observed vise versa, i.e. the pump beam intensity is amplified, whereas initially scattered light is depleted. This kind of amplification process holds for refractive index gratings, only, since photochromic effects generally show a local response. Amplification will occur in the case of a negative light-induced absorption in such media.

III. TYPES OF NON-LINEAR LIGHT SCATTERING

Non-linear light scattering can be divided into four different types, called wide-angle, matched, isotropic and anisotropic scattering, which reflect their essential physical properties. It should be noted, that all types can be combined with each other, so that the observation of a mixture of scattering phenomena is common. Examples of different combinations are given after a short description of each type.

- **wide-angle scattering:** Wide-angle scattering describes the scattering phenomenon, which is based on the simplest model for multi-wave interaction involving only two beams, i.e. recording and read-out beams coincide. In this special case, the Bragg-condition of the recorded parasitic grating is automatically fulfilled by the read-out beams, so that diffraction and beam-coupling occurs without restriction. Assuming a broad angular distribution of the seed scattering, a multitude of parasitic gratings will be recorded each having its very own Bragg-condition. Nevertheless, they all are automatically fulfilled by the pump beam, which results in a distribution of scattered light in a wide apex angle, which is the reason to call this phenomenon *wide-angle scattering*.

- **conical and parametric (matched) scattering:** In contrast to wide-angle scattering *matched scattering* describes the build-up of non-linear light scattering on the basis of wave interactions involving more than two waves. A characteristic feature of this scattering phenomenon is that the spatial distribution of the scattered light is limited and exhibits characteristic pattern, resulting from scattered light build from e.g. cones, rays or single beams. Depending on the nature of the multi-wave interaction we have to distinguish between conical and parametric (matched) scattering. Conical scattering describes all phenomena, where the scattered light propagates on the rim of a cone. Parametric scattering refers to processes analogue to four-wave mixing [54, 55], where true mixing between the waves takes place. Again, cones can be generated, but also beams. The origin of conical scattering can therefore be parametric as well as a result from deviated wide-angle scattering.

- **polarization isotropic and anisotropic scattering:** Linear polarized light is commonly used to induce non-linear light scattering in photorefractive materials. The scattering pattern are a result of the photorefractive processes, which may lead to a rotation of the light polarization by 90^o. If the light polarizations of scattered and incoming light are equal, the scattering phenomena is called *polarization isotropic* [37, 38], otherwise *polarization anisotropic* [19, 21, 56]. The latter is observed in polar oxides with non-diagonal elements of the dielectric tensor $\delta\epsilon_{ij}$. For example, anisotropic non-linear light scattering occurs in materials having only one non-vanishing non-diagonal element of the

tensor $r_{ijn}K_n$ [19, 21], with the electro-optic tensor component r_{ijn} and the grating vector K_n.

A. Polarization isotropic wide-angle scattering

Polarization-isotropic wide-angle light scattering is found in a multitude of photorefractive crystals [1, 9, 13, 21, 33, 43, 57–61] and shows a broad scattering scattering distribution beside the directly transmitted laser beam with a characteristic intensity profile (see Fig. 2).

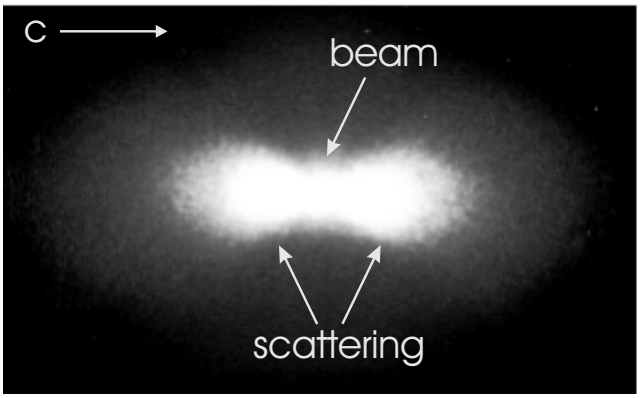

FIG. 2: Polarization-isotropic wide-angle scattering in $LiTaO_3$ observed on a screen behind the crystal. Two broad scattering distributions (lobes) appear in the steady state, which are oriented in and against the direction of the polar axis. $\lambda_p = 514.5$ nm, extraordinary light polarization.

Referring to the common explanation of non-linear light scattering the spatial intensity distribution can be described by the interplay between the spatial distribution of the seed scattering and the one of the amplification process. Assuming a symmetric intensity distribution of the initially scattered waves with respect to the pump beam, it is obvious, that an asymmetric nonlinear light scattering pattern will occur, if the amplification process shows specific directions of the maximum gain. This can especially be observed in polar electro-optic crystals, where the amplification process depends on the symmetry of the electro-optic tensor [22, 62, 63]. Purely asymmetric scattering pattern, as it is observed for strontium-barium-niobate (Figure 6), reflect the nonlocal photorefractive response and can therefore be analyzed by the application of the common model equations to the intensity distribution in the direction of the polar axis. This allows to determine model and material parameters, such as the distribution of the seed scattering and the electro-optic coefficients, respectively [64–66]. Further, polarization-isotropic wide-angle scattering is strongly dependent on external parameters, such as temperature [65] or the application of externally applied electric fields [64, 67], which allows to expand the determination of material parameters, as it is shown in detail for SBN below. The intensity distributions of polarization-isotropic wide-angle scattering can be found much more complicated in several polar oxides, e.g. two additional side lobes deviating from the c-axis direction are observed in $BaTiO_3$, which can be explained by elastic and piezoelectric properties [43]. As special observation of wide-angle scattering is made for $LiNbO_3$. Due to a non-local photorefractive response an asymmetric scattering pattern comparable to SBN is expected. However, this can be observed for extremely thick crystals (more than 7mm) [21, 37], only. In thin samples the scattering pattern shows two lobes, one in the direction of amplification and one even in the direction where depletion is expected [68]. A first attempt to explain this observation is given in [69]. Beside the polar oxides we have discovered polarization-isotropic wide-angle scattering in centrosymmetric NaNP [49]. Due to the centrosymmetric nature of the photorefractive effect the scattering pattern is found with a homogeneous intensity distribution in all directions of space.

B. Polarization-anisotropic wide-angle scattering

Polarization-anisotropic is observed especially in materials with the bulk photovoltaic effect as primary charge transport mechanism [54]. The basic requirement is a rotation of the light polarization of the reconstructed wave by 90^o in the diffraction process. Such phenomena have been discovered in $LiNbO_3$ [70] and $BaTiO_3$ [71] and arise after the build-up of pronounced polarization-isotropic wide-angle scattering. The sign of the photovoltaic tensor element needed for the polarization-flip is decisive for wether ordinary or extraordinary pump light is anisotropically diffracted. The comparison between $LiNbO_3$:Fe and $LiTaO_3$:Cu clearly shows, that extraordinary to ordinary processes are connected to a negative ($LiNbO_3$:Fe [72]) and vice versa to a positive photovoltaic tensor component ($LiTaO_3$:Cu [25]). An impressive phenomenon has been discovered in centrosymmetric sodiumnitroprusside, where polarization-anisotropic wide-angle scattering occurs as a broad and homogeneous distribution of scattered light [50]. In addition a sharp ring is observed, which is attributed to polarization-anisotropic matched scattering, as described below.

C. Polarization-isotropic conical scattering

Those cases where more than two plane wave components are involved in the generation of wide-angle light scattering can easily be recognized, since phase matching conditions apply in thick holographic media. They impose stringent restrictions on the scattering indicatrix of those processes and cause strikingly narrow structures in the scattering patterns as compared to the broad distributions characteristic for wide-angle scattering.

We first discuss conical matched scattering where one pair of waves interacts by a writing process and the sec-

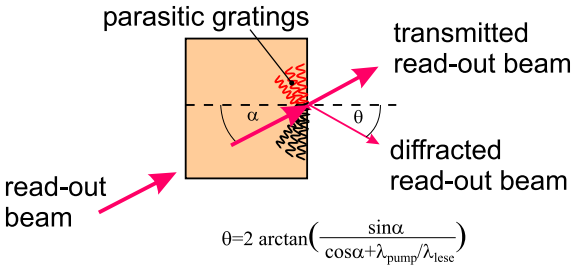

FIG. 3: Read-out of a recorded refractive index modulation results in diffraction processes, if the Bragg condition is fulfilled. In the case, that read-out and pump beams are identical, diffraction occurs at the complete set of recorded gratings (wide-angle scattering), else, i.e. if read-out wavelength or angle are deviated with respect to the pump beam, diffracted waves propagate on the rims of cone (conical scattering). The apex angle of such cones are directly connected to the used wavelength and read-out angle, as shown by the formula.

ond by a reading process on the same grating. Being interested only in the quasistatic excitations two processes are possible, called A and B processes [73]: the first corresponds to the reconstruction of the signal and the second of the (pseudoscopic) conjugate signal in the holographic read-out [74]. The Bragg conditions are fulfilled on the lines of intersection of Ewald's ellipsoid with the structure ellipsoids. As the intersection line of two ellipsoidal surfaces is always an ellipse, the scattered waves emerge on cones. This is why such type of scattering is called conical scattering. The "trivial case" of conical scattering is the one observed by simply detuning the angle of incidence of the pump beam after wide-angle non-linear light scattering had developed in a thick holographic recording medium [30, 31]. Thereby the Bragg condition is violated for all but the scattered wave vectors on the intersections of the Ewald ellipsoid with both structure ellipsoids and two ring-shaped bright patterns contrast on a screen behind the sample against the dark background. An impressing example of polarization-isotropic conical scattering is discovered in SNP, where both A and B process can be observed simultaneously (Fig. 4).

Sometimes the gain indicatrix or aperture limitations permit to see only one of these rings. Angular and wavelength dependence [30, 31, 75] as well as the diffraction fine structure [32] of the "trivial case" of conical scattering have been investigated. Trivial conical scattering is quite practical to analyse wide-angle non-linear light scattering or to unambiguously decide whether wide-angle scattering had occurred in a sample.

D. Polarization anisotropic parametric scattering

Parametric scattering describes phenomena where both pairs of waves are coupled by writing and reading. Note, that all scattering phenomena based on parametric four-wave processes are also conical and, therefore, a

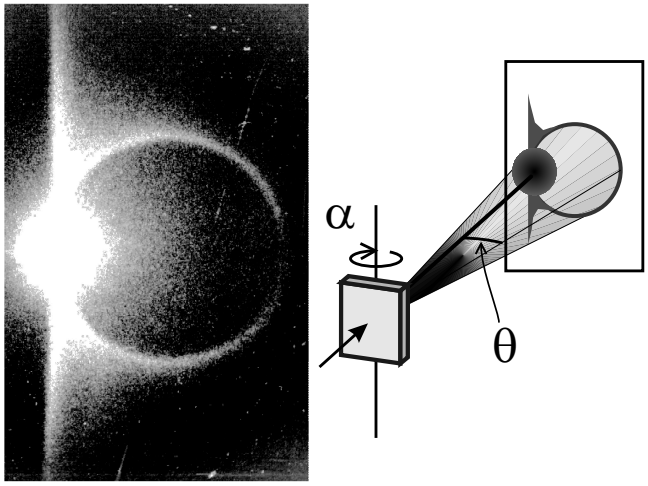

FIG. 4: Polarization-isotropic conical scattering in SNP. Both A and B-processes can be observed simultaneously as a sharp closed ring and a sharp ring-segment, respectively. Read-out has been performed with λ_r=514.5nm with an angular deviation of α=5^o. The apex angle θ is a function of read-out wavelength and angle (right part).

clear distinction between both phenomena from the experiment itself is doubtful. The existence of parametric light scattering showing ring structure is reported in several works [6, 21, 26, 27, 39, 40, 76, 77]. A special observation occurs, if two or more scattering cones intersect each other and thus single distinct beams occur, observable as characteristic "dots" on a screen [6]. Polarization anisotropic parametric scattering was discovered as bright cones of scattered light in $LiTaO_3$ [25, 48], $BaTiO_3$ and $LiNbO_3$ crystals [21, 26, 27, 56]. The apex angle of these scattering cones is dependent on the birefringence of the photorefractive crystal [21]. Polarization anisotropic parametric scattering can be observed even in centrosymmetric SNP [50]. An excellent review on parametric scattering is given in [73].

IV. PARAMETERS AFFECTING NON-LINEAR LIGHT SCATTERING

It is obvious, that non-linear light scattering is strongly influenced by a variety of parameters regarding the common model for this phenomenon [13]:

- type of the material used, including kind of dopants and doping concentration
- sample properties: thickness, optical quality of surface and volume
- incident laser beam: intensity, beam profile, orientation of the wave vector, light polarization, coherence length

However, there is an ongoing deep discussion about the origin of seed scattering. A first attempt is given in [78],

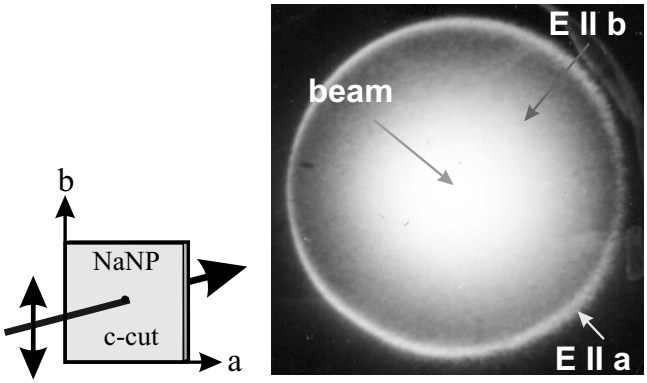

FIG. 5: Polarization-anisotropic parametric scattering in centrosymmetric sodiumnitroprusside (sharp ring) and polarization-isotropic wide-angle scattering (broad scattering corona).

assuming, that the main contribution to seed scattering is generated in the crystal volume in the vicinity of the surface: a) due the large change of the refractive index at the air-crystal boundary and b) due to strong extinction losses of the pump wave by absorption or scattering processes. In contrast, seed scattering was investigated by randomly distributed, screened charges in the volume of the crystal [23], which was based on the results of a computer simulations contradicting the model of surface seed scattering [79]. In addition to waves from scattering centers Forshaw considered waves diffracted at initially recorded phase gratings [32]. Obukhovskif et al. proposed the origin of seed scattering by static spatial fluctuations of the refractive-index and of the photovoltaic tensor [5, 80]. They also included static spatial fluctuations of the dark conductivity and of the tensor of photoconductivity [81]. Only recently, Goulkov demonstrated experimentally that refractive index perturbations located at ferroelectric domain tips are the origin of initial scattering especially in SBN [64].

A second fundamental requirement for the build-up of non-linear light scattering is the existence of an amplification process. A description of non-linear recording phenomena of surface and volume seed scattering is given by [24, 60], whereby the behavior of phase conjugated scattering is described in [82]. It was shown, that transient amplification takes place for the special case of a static seed scattering (e.g. Rayleigh noise or quasielastic scattering [82, 83]) in materials with a local photorefractive response [5]. Non-linear parametric phenomena have to be considered if scattering is created by two pump beams [35, 39, 41, 46, 76]. In many cases the temporal behavior of the non-linear scattering phenomena can be described by:

$$\frac{I_s(t)}{I_s(0)} = \frac{\exp(\Gamma_{\mathit{eff}}\ d) - 1}{\Gamma_{\mathit{eff}}\ d} \tag{1}$$

for scattered beams with intensity I_s [84] and by

$$\frac{I_p(t)}{I_p(0)} = \frac{1 + m_0}{1 + m_0 \exp(\Gamma_{\mathit{eff}}\ d)} \tag{2}$$

for the transmitted pump beam intensity I_p [21, 85]. Both formulae were derived from effective two-beam approximations [21, 86], where $\Gamma_{\mathit{eff}} = \Gamma[1 - exp(-t/\tau)]$ denotes the effective amplification, t the time, τ the effective relaxation time, and m_0 the initial scattering ratio. For the particular case of sillenites and fiber-like crystals with small electro-optic coefficients as compared to $BaTiO_3$ or SBN the diffusion-type photorefractive nonlinearity is small. The application of an alternating external electric field, in particular of square pulse form, may be used to achieve strong beam coupling and thus enhance light scattering [84]. It has been often overlooked that non-local recording does not necessarily mean recording by a diffusion field E_{diff} only. The complete expression for the non-local contribution E_{NL} to the space charge field is given by [87]:

$$E_{NL} = E_{\mathit{diff}} \frac{(1 + E_{\mathit{diff}}/E_q) + E^2/EqE_{\mathit{diff}}}{(1 + E_{\mathit{diff}}/Eq)^2 + E^2/E_q^2} \tag{3}$$

where E_q is the maximum space-charge field attainable for a given trap or donor density [88] and $E = E_0 + E_{ph}$. As the formula suggests, a constant photovoltaic field E_{ph} as well as a constant externally applied electric field E_0 enhance non-linear light scattering. The latter effect was not only experimentally demonstrated by direct application of an external field but by more subtly exploiting pyroelectric and depolarization fields generated by thermal and irradiation treatments [89]. As pointed out by Montemezzani et al., besides the properties usually considered (dielectric, conductive and electro-optic), in some cases piezoelectric and mechanical properties play a decisive role for amplification of light scattering [43]. Moreover, the importance of the wavelength of the recording beam, the angle of incidence [42], the crystal temperature [85], additional incoherent illumination [86], and the polarization of the recording beam [38, 90, 91] for the presence and strength of non-linear light scattering have been underlined by various authors. Angular and polarization dependencies discussed by Belendez et al. [92] might not originate from noise gratings but be caused by an optically induced birefringence of the medium. While no dependence of light scattering was found for beam diameters of 7 mm and 1 mm [58], Zhang et al. [61] report a decrease of light scattering for beam diameters below 0.9 mm, particularly striking for diameters below 15 μm where scattering vanishes. This was attributed to the decrease of the effective interaction length [22].

$$l_{eff} = L\left[1 - \exp\left(-\frac{D}{L\sin\theta}\right)\right] \quad (4)$$

for holographic amplification with decreasing beam diameter D at a given scattering angle θ and sample length L.

V. NON-LINEAR LIGHT SCATTERING IN SBN

The properties of non-linear light scattering and the respective impressing impact for material analysis can be clearly demonstrated at the example of the polar oxide strontium-barium-niobate, $Sr_{0.61}Ba_{0.39}Nb_2O_6$ (SBN61), which shows a non-local photorefractive response due to diffusion processes [93] and features large linear electro-optic coefficients [94, 95]. We will therefore summarize the latest experimental results and analysis of non-linear light scattering in more detail especially for this material. A characteristic steady-state far-field scattering pattern is shown in Fig. 6. Strongly amplified scattered light is observed in one direction beside the directly transmitted pump beam. The laser beam propagates through a crystallographic a-cut normal to the crystal surface and an extraordinarily light polarization.

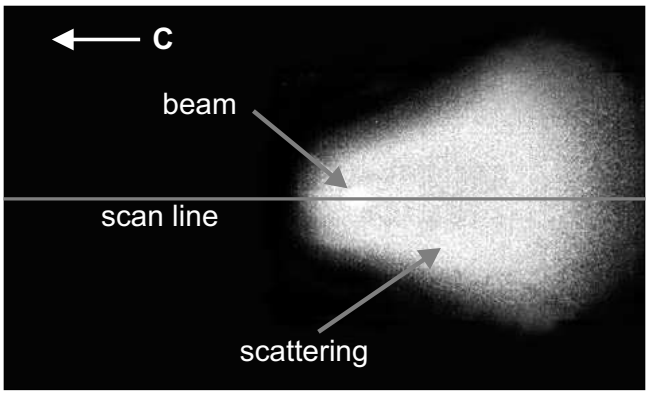

FIG. 6: Polarization-isotropic non-linear wide-angle scattering in strontium-barium-niobate doped with o.66 mol% cerium (SBN61:Ce). Strongly amplified scattered light occurs in a direction opposite to the polar c-axis. λ_p=632.8nm, $\mathbf{E} \parallel c$.

The asymmetric scattering pattern and its distribution originates from the angular dependence of the holographic gain $\Gamma(\theta)$. Hereby, amplification occurs against and depletion in direction of the polar c-axis since electrons are the dominating charge carriers. A detailed study of transport models and photo-ionization processes can be found in [96, 97]. The gain is proportional to the effective linear electro-optic coefficient $r_{eff}(T)$ and the space charge field $E_{sc}(T)$, which depends on the scattering angle $\theta(T)$ due to the temperature dependent screening length [98]: $\Gamma \approx r_{eff}(T)E_{sc}(\theta(T))$. Therefore, the intensity distribution of the scattered light is a function of temperature, i.e. the behavior of linear electro-optic coefficients and space charge fields can be studied by non-linear light scattering, as will be shown in detail below. In addition, non-linear light scattering can be used to investigate the critical relaxor-kind phase transition in SBN [99], which executes from the tetragonal polar point symmetry group 4mm to the 4/mmm high temperature phase at about T = 360 K [100]. The phase transition temperature depends strongly on the doping element and concentration [101, 102], whereby Ce^{3+} occupies Sr^{2+} sites in off-center positions [103, 104]. This kind of a phase transition is characterized by a non-vanishing spontaneous ferroelectric polarization above the transition temperature, which can be explained by a random field Ising model [105, 106]. Here, random fields act as pinning centers for the ferroelectric polarization, so that clusters of non-zero spontaneous polarization survive in the paraelectric regime decaying over a large temperature range. It should be noted, that the electro-optic coefficient is proportional to the spontaneous polarization, so that an inversion of the direction of the polar axis by externally applied electric fields results in an inversion of the amplification direction of the scattering pattern. This property can be used to measure the ferroelectric hysteresis behavior [64], as shown below. In the following, the common explanation for non-linear light scattering is assigned to the charge transport mechanism and amplification processes, which are valid for SBN.

A. Basic model for polarization-isotropic wide-angle scattering in SBN

Polarization-isotropic wide-angle scattering from a single pump beam is usually interpreted as a result of nonlinear two-beam coupling between scattered and transmitted parts of the incident beam [9, 93]. We will describe this process within a simplified photorefractive model assuming the following model parameters.

- diffusion of photocarriers is the dominating charge transport mechanism in SBN in the absence of an external electric field, since the photovoltaic effect is extremely small in SBN:Ce [96] at the temperatures used in the experiment;
- electrons are the major contributors to photoinduced currents [107], and the influence of positive charge carriers (holes) can be neglected;
- an undepleted pump approximation [98, 108] can be used in the case of the comparatively weak light-induced scattering;
- the absorption coefficient for SBN:Ce ($\alpha = 4$ cm^{-1} at λ=632nm) is approximated to zero in order to simplify the model equations and the numerical treatment of the experimental results.

The pump beam propagates in the crystal and is partially scattered on optical inhomogeneities and imperfections in the sample. This initial optical noise consists of plane seed waves propagating at different angles θ_s from the direction of the pump beam. The seed wave s interferes with the pump wave p and forms an elementary light interference pattern

$$I = I_0[1 + m\cos(\mathbf{K}\cdot\mathbf{r})] \tag{5}$$

with a spatial period of $\Lambda{=}\lambda/2\sin\theta_s{=}2\pi/K$, where λ is the wavelength of the incident light, $\mathbf{K}$ is the grating vector of the light modulation, $m{=}2\sqrt{I_s\cdot I_p}/I_0$ is the modulation depth and $I_0{=}I_s{+}I_p$ the total intensity of the recording beams. Due to processes of thermal diffusion (and drift in an externally applied field), photoexcited electrons migrate from bright to dark regions and yield the periodically modulated space-charge field

$$E_{sc}(\mathbf{r}) = mE^o_{sc}\cos(\mathbf{K}\cdot\mathbf{r}+\mathbf{\Phi}), \tag{6}$$

where E°_{sc} is the amplitude of the spatially varying field and Φ its phase shift with respect to the incoming light interference pattern [108, 109]. In the case of SBN the phase shift is always exactly $\Phi{=}90°$ when there is no externally applied electric field ($E_o{=}0$). In the experiments described below, where $E_o \neq 0$, a change of the phase shift Φ of up to 5% results, which can be neglected. The increase of the space charge field at the maximum field strength of $E_o{=}$ 4kV/cm is only 15% in comparison to zero field.

The linear electro-optic effect transfers the electric charge grating into a refractive index grating:

$$\begin{aligned}\Delta n(\mathbf{r}) &= (\Delta n)_o\sin(\mathbf{K}\cdot\mathbf{r}) \\ &= -\frac{1}{2}r_{\mathit{eff}}n^3_{\mathit{eff}}E^o_{sc}\sin(\mathbf{K}\cdot\mathbf{r})\end{aligned} \tag{7}$$

where n_{eff} is the effective refractive index and r_{eff} is the effective electro-optic coefficient. The spatial $\Lambda/4$-shift between the refractive grating and the light pattern causes an effective stationary energy exchange between pump and seed waves, resulting in an exponential change of the intensity of the seed wave: $I_s(d) = I_{so}\exp(\Gamma d)$, where d is the crystal thickness, and the exponential increment

$$\Gamma = \frac{4\pi(\Delta n)_o}{\lambda\cos\theta_s} \tag{8}$$

is the gain coefficient describing the efficiency of the direct coupling between the waves p and s. When using the corresponding expression for the amplitude of the diffusion field [109] and taking into account the particular conditions of our experiment, the coupling coefficient Γ can be written for the polarization-isotropic wide-angle scattering in SBN as:

$$\Gamma(\theta_s,T) = \mp\frac{2\pi n_e^3\zeta r_{33}}{\lambda\cos\theta_s}\frac{k_BT}{e}\frac{K}{1+(K/K_D)^2}, \tag{9}$$

where e is the elementary electric charge, k_B is Boltzmann's constant and T is the absolute temperature. The inverse Debye-screening length K_D is given by $K_D{=}\sqrt{e^2N_{eff}/(\varepsilon_{33}\varepsilon_o k_BT)}$, ε_{33} and ε_o are the dielectric constants of SBN and free space, respectively. $\zeta \leq 1$ is introduced to account for electron-hole competition. The effective trap density N_{eff} is measured to $2.2{\times}10^{23}$ m^{-3} for SBN doped with 0.66 mol% Cerium [110]. The sign of r_{33} was measured to be positive [110, 111]. Hence, the scattering propagating in the $-c$-direction (positive Γ) is amplified, and in the $+c$-direction (negative Γ) is depleted, resulting in the strongly asymmetric scattering pattern shown in Fig.6.

Here we have to note that the effect of the external electric field can not be reduced only to small changes of E^o_{sc} and Φ values. High electric fields E_o larger than the coercive field E_c should result in a spatial inversion of the macroscopic polarization P_s of the sample and in a corresponding inversion of the sign of the gain coefficient Γ (see hysteresis behavior below).

B. Angular dependence

The experimental setup used for our investigations is shown in figure 7.

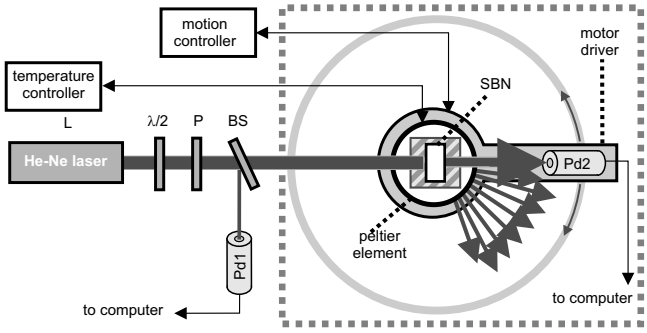

FIG. 7: Experimental setup for measuring the angular distribution of the scattered light at different temperatures and externally applied electric fields. L is a He-Ne-laser, $\lambda/2$ a half-wave retarder plate, P a Glan-Thomson prism, BS a beam splitter, PD1 and PD2 are photodiodes. The SBN61:Ce (0.66 mol%)sample is placed on a stack of Peltier-elements to regulate the temperature.

The beam of a low-power He-Ne-laser (5mW) serving as the pump beam with a wavelength of λ=632.8 nm was directed normal to the large a-surface of the sample with $\mathbf{E} \parallel c$. The intensity of the pump beam was adjusted to 70 mW/cm^2 using a half-wave retarder plate and a Glan-Thomson prism in order to prevent nonlinear effects other than light-induced scattering. The pump beam had a Gaussian intensity distribution with a

FWHM of 0.8 mm. A small fraction of the pump beam was directed to a photodiode PD1 by a beam-splitter BS to monitor the laser intensity. Photodiode PD2 was placed behind the sample at a distance of 5.5 cm and was mounted on a rotation stage driven by an electronic motion controller. When moving, photodiode PD2 made an exact half-circle around the sample in the direction from the negative to the positive end of the polarization vector in order to measure the light distribution in the plane of incidence parallel to the c-axis. The scattered light is measured in the angular range -90$^o \leq \theta_s \leq$+90^o, where the negative and positive scattering angles θ_s correspond to the scattering against and along the direction of the polar c-axis, respectively. At θ_s=0^o the photodiode crosses the pump beam directly behind the crystal. The aperture of the diaphragm on PD2 limits the apex angle of the measured scattered light to 0.5^o. The entire setup is enclosed in a black box (represented by the dotted rectangle in the figure) with only a small opening for the pump beam to minimize the noise due to external light sources. To obtain a baseline curve, the intensity distribution of the laser was measured without a sample in the holder. For our investigations we used a single crystal of SBN61 doped with 0.66 mol% Cerium. It was grown by the Czochralski technique by R. Pankrath from the crystal growth department of Osnabrück and cut parallel to the crystallographic axes into a rectangular parallelepiped with dimensions of 0.90×7.15×6.20 mm^3 along the a-, b- and c-axis, respectively. The temperature of the phase transition between the paraelectric and the ferroelectric state is found at T=52^{o}C [66]. The sample was poled by heating up to 140 ^{o}C, applying an external electric field of 350 V/mm along the crystallographic c-axis and then slowly cooling down to room temperature before removing the field. This procedure results in a sample where practically all existing domains are aligned according to the external field [112]. Then the sample was placed in a holder and fixed on a thermoelectric element. A temperature controller allowed to adjust the sample temperature from 10^{o}C to 150^{o}C with an absolute accuracy of 0.3^{o}C. The faces of the sample normal to the crystallographic c-axis were short circuited to prevent an influence of pyroelectric fields when the sample temperature was changed. An high voltage amplifier was used for measurements with externally applied electric field. The maximum amplitude was pm3.5kV, which could be adjusted with a 12 bit resolution.

Fig. 8 shows the one-dimensional angular profile of the steady-state intensity distribution of this pattern (crystal temperature is T=28 °C) as a solid curve (a). The sharp intensity peak in the central part of the scan corresponds to the directly transmitted pump beam. Because of the small aperture of the diaphragm on the photodiode PD2, this peak is only a section of the beam cut by the diaphragm. The dashed curve (b) represents the angular profile of the pump beam without the sample. Both intensity profiles are normalized to their maximum intensities I_{max}. The angular distribution of the light pattern

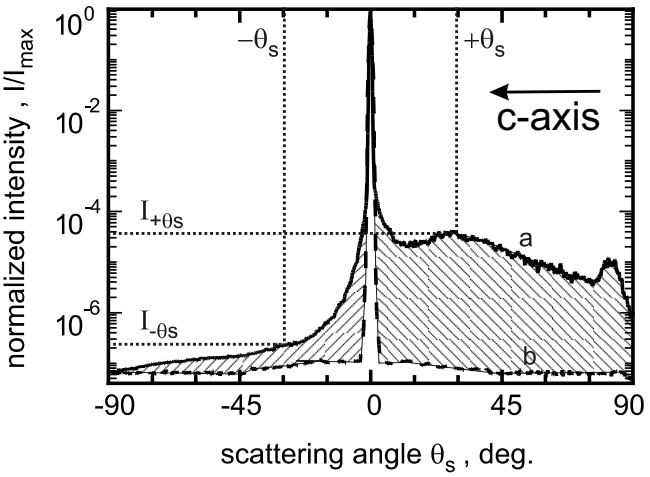

FIG. 8: a) Typical angular distribution of the scattered light in SBN at T=28^{o}C in the plane spanned by the $c-$axis and the laser beam. The central peak is the transmitted laser beam. The two crosshatched areas to the left and to the right of the peak are taken to derive the integral intensities in the $-c$ and $+c$ directions of the scattering profile, respectively. The intensities $I_{+\theta s}$ and $I_{-\theta s}$ correspond to two symmetric scattering angles, where $\pm\theta s$ is defined by the maximum of the intensity of the scattering pattern. b) Beam profile without a sample, representing the noise of the system.

as well as the pattern on the photo in Fig. 6 are strongly asymmetric: The main part of the scattered light is found at positive scattering angles θ_s, corresponding to the direction opposite to the c-axis ($-c$-direction). The scattering in the $-c$-direction exhibits a wide and not well pronounced maximum at the angle $\theta_s^{I_{max}}$=(30±5) °. The scattering measured along the c-axis (negative scattering angles or $+c$- direction) is rather weak. To get a quantitative measure of this asymmetry of the scattering distribution, we introduce the asymmetry coefficient m_{as}=I_{-c}/I_{+c} defined as the intensity ratio of the scattering in the $-c$-direction and in the $+c$-direction. I_{-c} and I_{+c} are the integral scattering intensities in the $-c$- and $+c$-directions measured in the steady state and shown in Fig. 8 by the two crosshatched areas below the intensity curve. The angular interval $-2° \leq \theta_s \leq 2°$ is excluded from the calculation of I_{-c} and I_{+c} in order to take into account the scattered light only. The measured asymmetry coefficient for the scattering profile shown in Fig. 8 is m_{as}=14.3.

C. Temperature dependence

In the following we will present the behavior of nonlinear light scattering as a function of the temperature [66]. The study of the spatial distribution of the intensity of the scattered light was carried out at different temperatures in the range from +15° to +148° . Fig.9 shows three beam-fanning profiles measured with the same SBN sample at different temperatures: Curve

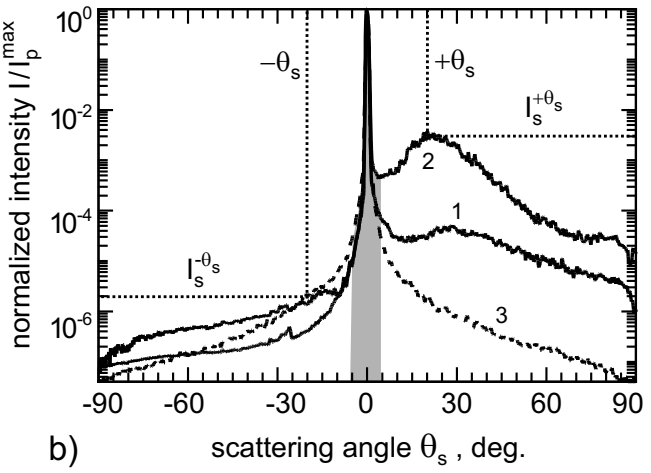

FIG. 9: Angular distributions of scattered light measured along c-axis at zero external field and different temperatures: T=28°C (curve 1), T=52°C (curve 2) and T=130°C (curve 3). The central peak corresponds to the directly transmitted pump beam. The shadowed area displays the angular interval influenced by transmitted pump beam.

1 is for T=28°C (ferroelectric phase), curve 2 is for T=52°C ($T \approx T_c$) and curve 3 is for T=130°C (paraelectric phase). The central intensity peak at θ_s=0° is formed by the transmitted pump beam (the shadowed area marks the angular interval where the pump peak influences the scattering distribution). The basic properties of the temperature dependence of non-linear light scattering in SBN are:

- If SBN is in the ferroelectric phase, the scattering pattern is strongly asymmetric, and most of the scattered light is observed in the direction opposite to the c-axis of the crystal (positive scattering angles θ_s in Fig.9).

- Due to a strong temperature dependence of the beam coupling process, heating the crystal up to T_c=52°C significantly increases the total scattering intensity and at the same time makes the asymmetry of angular light distribution more pronounced.

- Because of the relaxor behavior of SBN [18, 19], quite strong light-induced scattering is observed even at $T > T_c$ due to the presence of polar clusters.

- In the paraelectric phase at $T \gg T_c$, where polar clusters vanish and no beam-coupling is possible because the polar macrostructure is no longer present, only the weak seed scattering is observed. Due to the drastic changes in the domain structure at the phase transition, the seed scattering at 130°C differs from that at 28°C both in the total amount and in the angular distribution.

These properties demonstrate that the study of nonlinear light scattering can be used to investigate the relaxor-kind phase transition by an optical method. Hereby, various measures can be used, like the temperature dependence of the intensity of the directly transmitted laser beam, of the integrated scattered light and of the asymmetry coefficient, respectively, as it is shown in Figs. 10 and 11.

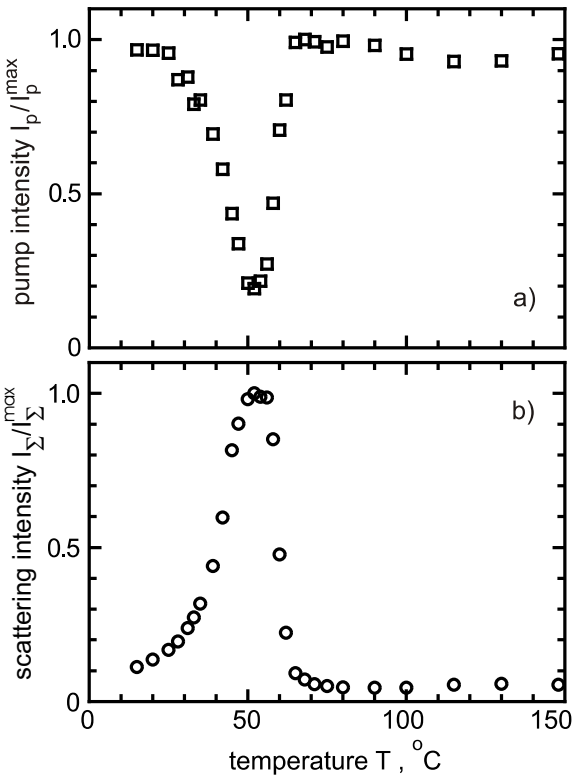

FIG. 10: a) Temperature dependence of the transmitted pump intensity. b) Temperature dependence of the total scattered intensity $I_\Sigma = I_- + I_+$. Both curves have been normalized to their maximum values.

Fig. 10a shows the transmitted pump intensity $I_p(T)$, Fig. 10b shows the integrated intensity $I_\Sigma(T)$=$I_-(T)$ + $I_+(T)$ of the scattered light obtained from the angular scan. In order to show only the temperature dependence of the curves, they have been normalized to their maximum values. Fig. 11 shows the temperature dependence of the asymmetry coefficient m_{as} over the whole temperature range. In the first phase from low temperatures to about 52 °C, the total scattered intensity increases nonlinearly. Additionally, the transmitted pump beam decreases. The intensity of the scattering grows in the $-c$-direction and drops in the $+c$-direction, leading to a sharp increase of the asymmetry coefficient. The second phase begins at T $\geq$ 52 °C and continues up to about T=65 °C. In this phase, the total scattering intensity starts to decrease, while the intensity of the transmitted pump beam increases. The decrease of the scattered intensity is especially pronounced for large angles in both directions, while the scattered intensity for small angles still shows a large maximum. In this phase, the fast

decay of the asymmetry of the scattering pattern takes place, the intensity I_{-c} decreases and I_{+c} increases, resulting in a very pronounced maximum of the asymmetry coefficient. The scattering intensity and the asymmetry coefficient are reduced to the values comparable to those at room temperature. At T=65 °C, the third and last phase of the temperature development of the scattering starts. The transmitted pump intensity continues to increase and the total scattered intensity continues to decrease, but at a much slower rate than in the previous phase. At T=100 °C the photo-induced scattering practically vanishes into the background noise. The asymmetry coefficient in the third phase becomes much smaller compared to the values at room temperature and finally falls to unity for T≥100 °C, indicating an absolutely symmetric angular distribution of the scattered light. This phase of the temperature evolution of the scattering is illustrated by slow tails of the curves in Figs 10 and 11. It should be noted that the scattering exhibits a reversibility with respect to the heating and cooling procedures: When the crystal is cooled back to room temperature, the scattering maximum reappears and the light pattern becomes asymmetric again. The evolution of the scattering in this case passes the above mentioned three phases in reverse order.

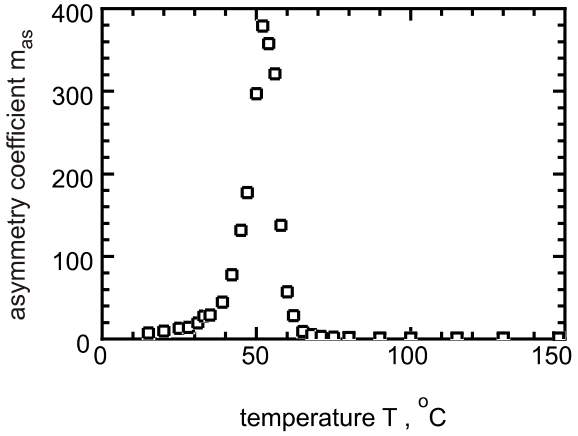

FIG. 11: Dependence of the asymmetry coefficient $m_{as} = I_-/I_+$ on the temperature.

These results clearly demonstrate that the relaxor-kind phase transition strongly influences the appearance of non-linear light scattering and, therefore, its temperature dependence can be used as a method for optical investigation of phase transitions. E.g. the transition temperature can be determined by the asymmetry parameter as a measure for the symmetry of the scattering pattern or by the comparable simple measurement of the directly transmitted laser beam.

D. Determination of Γ, ($\zeta \cdot r_{eff}$) and N_{eff}

The scattering pattern contains additional information about the scattering process itself as well as for the determination of material parameters. We will demonstrate in the following, that both the angular dependence of the holographic gain (scattering property) and the effective linear electro-optic coefficient in product with the electron-hole competition factor and the effective trap density (material properties) can be determined from the spatial distribution of the scattering pattern even as a function of the temperature [65].

We assume that the intensity of the primary scattered light from a single scattering center is the same for both directions θ_s and $-\theta_s$. It has to be noted that this assumption does not imply that the intensity distribution of the primary scattered light is homogeneous [64]. The values of Γ for two symmetric angles θ_{s1} and $\theta_{s2} = -\theta_{s1}$ differ only in sign, thus taking the logarithm of the corresponding ratio of the two scattered intensities $I_{\theta_{s1}}=I_0 \exp(+|\Gamma|_{-c} l)$ and $I_{\theta_{s2}}=I_0 \exp(-|\Gamma|_{+c} l)$ will give us twice the absolute value of the two beam coupling gain:

$$2\,|\Gamma|\,l = \ln(I_{\theta_{s1}}/I_{\theta_{s2}}) \tag{10}$$

Figure 12 shows the calculated values of $|\Gamma|$ versus the scattering angle θ_s for T=20,^{o}C (circles), T=45^{o}C (squares) and T=65^{o}C (crosses).

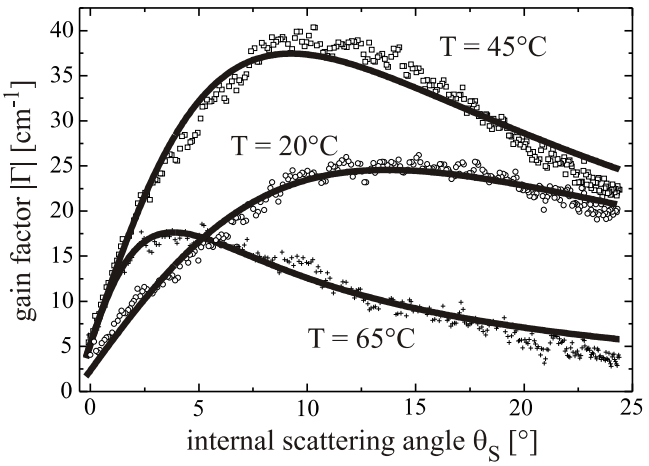

FIG. 12: Absolute value of the two beam coupling gain Γ versus the scattering angle θ for T=20^{o}C (circles), T=45^{o}C (squares) and T=65^{o}C (crosses). The solid lines are fits according to eq.8.

The figure shows only the coefficient Γ_{-c} corresponding to the −c-direction. Note that the internal scattering angle θ_s^{in} displayed in this figure ranges from about $0^o \leq \theta_s^{in} \leq 25^o$, corresponding to externally observed angles in the range of $0^o \leq \theta_s^{out} \leq 90^o$, due to the large refractive index of n_e=2.281 [113]. Now, equation 8 can

be fitted to the experimental data, which allows to determine the effective electro-optic coefficient r_{eff} and the effective trap density N_{eff} since the material parameters n_e and ϵ_{33} are known at different temperatures [114–116]. Fits are represented by the continuous lines in Figure 12. The very good result of the fitting procedure performed on the Γ- curves is apparent and shows that the simple model considered above describes the angular distribution of the beam fanning in SBN quite successfully. At the same time, one should note that the accurate fitting of the original I_s-curves is not possible without knowledge of the angular behavior of the seed scattering I_s^0. As it is mentioned above, the initial scattering exhibits a very strong dependence on the angle θ_s [64], and this can essentially influence the real intensity distribution from sample to sample. Our method of separate extraction of Γ- and I_s^0-curves allows to solve this problem. Moreover, the determination of an angular dependence of the coupling coefficient Γ in SBN from the scanned light-induced scattering distribution is much easier than that from the two-beam coupling experiment: we do not need to rearrange the setup to measure Γ for every new angle.

The extraction made from Figure 12 for T=20^{o}C gives ζr_{33}=(324±16)pm/V. In comparison, the standard interferometric method gives the value of electro-optic coefficient also measured at T=20^{o}C and for the same SBN sample as r_{33}=(354±2)pm/V [117]. Thus, one can deduce that the electron-hole competition is $\zeta \approx$(0.92±0.04) and the product ζr_{33} can be substituted by only r_{33} with a quite high accuracy. It is obvious, that this analysis can be performed for different temperatures, so that the determination of the mentioned parameters is possible as a function of the temperature with a sufficient high accuracy.

The advantage of this method is apparent, when compared to commonly used holographic or interferometric setups. At first the complexity of the experimental setup is marginal and the requirements to the mechanical stability are negligible. The second point belongs to the effort which is necessary to determine the desired parameters. In holographic two-beam coupling experiments the recording beams have to be adjusted for each single Bragg angle θ, whereas the complete angular range over 180° is directly determined by the steady state intensity distribution of the scattering pattern.

E. Hysteresis behavior

We will demonstrate in the following, that non-linear light scattering can be used for the optical determination of the ferroelectric hysteresis behavior as well [64]. Instead of the detection of the ferroelectric polarization P by measuring the surface charge per area, the optical determination by non-linear light scattering is based on the determination of the asymmetry parameter as a function of the externally applied electric field. The fundamental physical relation is given by the dependence of the amplification direction of the seed scattering on the direction of the polar axis. To explain a spatial switching of the scattering pattern and the hysteresis-like behavior of the asymmetry parameter m_s in SBN under an external electric field, one should consider the correlation between the photorefractive effect and the spontaneous polarization of the crystal. The linear electro-optic coefficient r_{33} depends on the macroscopic polarization P_s as follows [118]:

$$r_{33} = 2g_{33}P_s\varepsilon_{33}\varepsilon_0, \tag{11}$$

where g_{33} is the quadratic electro-optic coefficient. An inversion of the vector of the spontaneous polarization changes the sign of r_{33} in Eq.(11). This in turn causes a change of the sign of the gain factor Γ in Eq.(8) and results in the spatial inversion of the beam-fanning.

The procedure to determine the scattering hysteresis was performed as follows: The external field E_o is applied to the crystal without any illumination for a duration of 10 seconds. Then it is switched off. After a relaxation time of 1-2 minutes, which is long enough to reach the steady state of the spontaneous polarization in SBN [28], the crystal is illuminated with the pump beam. The asymmetric scattering pattern builds up, its angular distribution is investigated in the steady state.

Figs. 13a,b show the experimental results of the electric field dependency of the coefficient m_s and the scattering intensity I_s normalized on zero-field intensity. Note that the definition of the asymmetry parameter has been slightly changed by a normalization to the totally scattered light.

Arrows indicate the direction of the change of E_o during the experiment. It can be seen from Fig. 13a that when the external field is going from −4 kV/cm to positive values, the coefficient m_s remains unchanged until a field of E_o=+1.2 kV/cm is exceeded. Then it reverses its sign back to positive and approaches a value of m_s=0.96 measured at E_o=+4 kV/cm. The value E_o at which the m_s-curve crosses the abscissa is different for descending (left) and for ascending (right) parts of the scattering hysteresis. This allows us to evaluate the coercive field E_c to be 1.53 kV/cm and 1.22 kV/cm if the external field is anti-parallel and parallel to the initial direction of P_s after the poling of the sample at high temperatures, respectively. At the same time, according to Fig.13b, the total scattering intensity increases slightly at high negative fields (after E_o=−4 kV/cm), saturates near to a zero field, then drops into the next minimum at $E_o \approx +1.3$ kV/cm. It then increases again at high positive fields. When the externally applied electric field is finally reduced to zero, the coefficient m_s remains nearly constant, the total scattering intensity arrives at a value which is higher by a factor of 2.2 than that of the starting point. The hysteresis-like behavior of $m_s(E)$ indicates the ability of the non-linear light scattering to reverse its orientation in space perfectly when the external field is applied to the SBN sample.

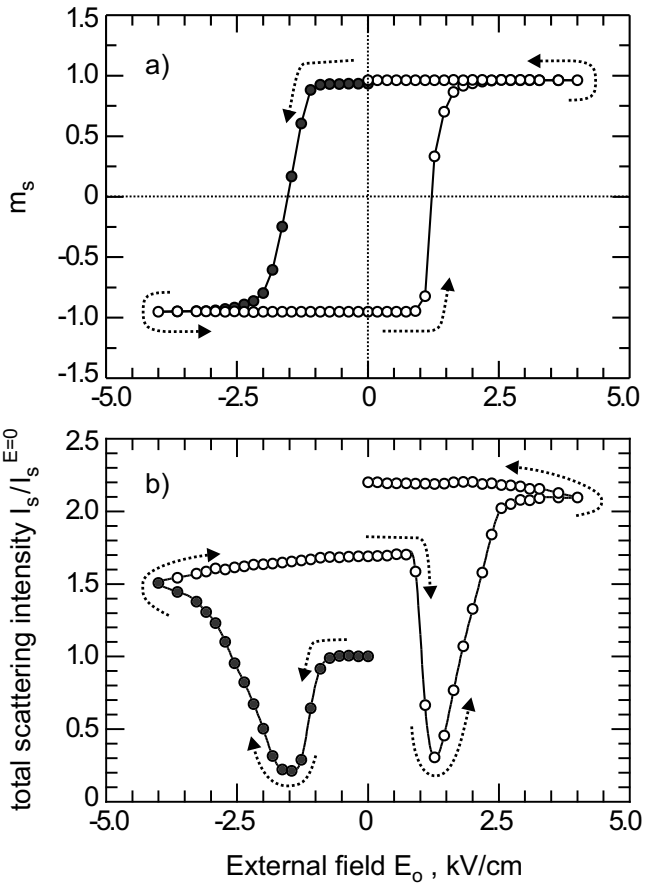

FIG. 13: Results of a scattering hysteresis experiment with an external electric field E_o: *a*) coefficient m_s=$(I_- - I_+)/(I_- + I_+)$ versus E_o; *b*) total scattering intensity I_s normalized on zero-field scattering intensity versus E_o. Arrows shows how the field is changed.

The different values of E_c found on the descending (left) and the ascending (right) parts of the m_s-E hysteresis can be attributed to the memory effect appearing in the field-cooled samples. During the poling procedure strong internal fields are induced in the crystal volume at high temperatures by the external field E_o and then frozen during the cooling process. These fields cause a predisposition of the macroscopic polarization to assume its initial orientation if the crystal then is repeatedly repoled by an alternating external field at low temperature. A similar memory effect has been observed in measurements of the ferroelectric hysteresis [112].

From the general relation equation (11) between the linear electro-optic effect and the spontaneous polarization of a photorefractive crystal, we have shown qualitatively that the light-induced scattering hysteresis is unambiguously defined by the relevant P_s-E hysteresis. Quantitative consideration of this question requires further developing of the model of photorefractive scattering, particularly a separate study of the origin of the seed scattering (primary scattering I_{so}) and the subsequent process of nonlinear amplification (gain coefficient Γ) of the scattered light.

VI. SUMMARY

In this work we have summarized the most important properties of non-linear light scattering, the corresponding basic notations and nomenclature. The origin of this effect is described on a common model based on multi-wave interaction and the recording of parasitic phase gratings. Some recent results especially obtained for SBN are summarized. To account for the increasing popularity of methods in materials research these results are presented in the frame of applicability for the determination of material parameters and properties.

ACKNOWLEDGEMENTS

This work was supported by the Deutsche Forschungsgemeinschaft (GRK 549/1-99), (SPP 1056 Wo 618/3-3).

[1] Ashkin, A., Boyd, G. D., Dziedzic, J. M., Smith, R. G., Ballman, A. A., Levinstein, A. A., Nassau, K., Appl. Phys. Lett. **9**, 72 (1966)
[2] Chen, F. S., la Macchia, J. T., Fraser, D. B., Appl. Phys. Lett. **13**, 223(1968)
[3] Chen, F. S., J. Appl. Phys. **40**, 3389 (1969)
[4] Stepanov, S. I., Reports on Progress in Physics **57**, 39 (1994)
[5] Obukhovski, V. V., Stoyanov, A. V., Opt. Spectros.(USSR) **58**, 226(1985)
[6] Goul'kov, M. Y., Odoulov, S. G., Sturman, B. I., Chernykh,A. I., Kratzig, E., Jakel, G., J. Opt. Soc. Am. B **13**, 2602 (1996)
[7] Kamber, N. Y., Xu, J., Mikha, S. M., Zhang, G.,Liu, S., Zhang, G., Opt. Commun. **176**, 91 (2000)
[8] Zozulya, A. A., Anderson, D. Z., Phys. Rev. A **52**, 878 (1995)
[9] Feinberg, J., J. Opt. Soc. Am. **72**, 46 (1982)
[10] Banerjee, P. P., Misra, R. M., 1993. Opt. Commun. **100**, 166 (1993)
[11] Liu, J.-J., Banerjee, P. P., Song, Q. W., J. Opt.Soc. Am. B **11**, 1688(1994)
[12] Odoulov, S., Tarabrova, T., Shumelyuk, A., Naumova, I. I.,Chaplina, T. O., Phys. Rev. Lett. **84**, 3294 (2000)
[13] Kanaev, L. F., Malinovsky, V. K., Sturman, B. I., Opt. Commun. **34**, 95 (1980)
[14] Wang, F., Liu, L., Yan, X., J. Mod. Opt. 45, 1645 (1998)
[15] Jullien, P., Mathey, P., Lompre, P., Odoulov, S., Sturman,B., J. Opt. Soc. Am. B **15**, 2018 30(1998)
[16] Odoulov, S. G., Soskin, M. S., in Photorefractive Materials and their Applications II, Vol. 62 of Topics in applied physics, edited by Gunter, P., Huignard, J.-P., (Springer-Verlag, Berlin, Heidelberg, New York, 1989), Chap. 2, pp. 5-43.

[17] Gunter, P., Huignard, J.-P., in Photorefractive Materials and their applications I, Vol. 61 of Topics in applied physics, edited by Gunter, P., Huignard, J.-P., (Springer-Verlag, Berlin, Heidelberg New York, 1987), pp. 7-70.
[18] Khuktarev, N. V., Markov, V. B., Odulov, S. G., Soskin, M. S.,Vinetskii, V. L., Ferroelectrics **22**, 949(1979)
[19] Avakyan, E. M., Belabaev, K. G., Odulov, S. G., Sov.Phys. Solid State **25**, 1887 (1983)
[20] Grousson, R., Mallick, S., Odoulov, S., Opt. Commun. **51**, 342 (1984)
[21] Rupp, R. A., Drees, F. W., Appl. Phys. B **39**, 223(1986)
[22] Valley, G. C., J. Opt. Soc. Am. B **4**, 14 (1987)
[23] Gu, C.,Yeh, P., Opt. Lett. **16**, 1572 (1991)
[24] Segev, M., Engin, D., Yariv, A., Valley, G. C., Opt. Lett. **18**, 956 (1993)
[25] Odoulov, S., Belabaev, K., Kisleva,I., Opt. Lett. **10**, 31 (1985)
[26] Temple, D. A., Warde, C., J. Opt. Soc. Am. B **3**, 337 (1986)
[27] Ewbank, M. D., Yeh, P., Feinberg, J., Opt. Commun. **59**, 423(1986)
[28] Rupp, R. A., Marotz, J., Ringhofer, K. H., Treichel, S.,Feng, S., Kratzig, E., IEEE J. Quant. Electron. QE-23, 2136 (1987)
[29] Prudkovski, P. A., Skugarevski, O. V., Optics and Spectroscopy **82**, 464(1997)
[30] Moran, J. M., Kaminow, I. P., Appl. Opt. **12**, 1964 (1973)
[31] Forshaw, M. R. B., Appl. Opt. **13**, 2 (1974)
[32] Forshaw, M. R. B., Opt. Commun. **15**, 218 (1975)
[33] Phillips, W., Amodei, J. J., Staebler, D. L., RCA Rev. **33**, 94 (1972)
[34] Zhang, G., Li, Q. X., Ho, P. P., Alfano, R. R., J. Opt. Soc. Am. B **4**, 882(1987)
[35] Sturman, B.,Goulkov, M., Odoulov, S., Appl. Phys. B **56**, 193(1993)
[36] Goul'kov, M. Y., Odoulov, S. G., Sturman, B. I., Appl. Phys. B **56**, 223(1993)
[37] Fally, M., Ellabban, M. A., Rupp, R. A., Fink, M., Wolfsberger, J., Tillmanns, E., Phys. Rev. B **61**, 15778 (2000)
[38] Ellabban, M. A., Rupp, R. A.,Fally, M., Appl. Phys. B **72**, 1(2001)
[39] Odoulov, S., Sturman, B., Holtmann, L., Kratzig, E., Appl. Phys. B **52**, 317 (1991)
[40] Novikov, A., Odoulov, S.,Jungen, R., Tschudi, T., Opt. Lett. **16**, 1941(1991)
[41] Sturman, B., Odoulov, S., Holtmann, L., van Olfen, U., Appl. Phys. A **55**, 65 (1992)
[42] Li, G., Yang, T., Teng, Y. Y., Lin, F. C., Fiddy, M. A., Waves in Random Media 2, 303 (1992)
[43] Montemezzani, G., Zozulya, A. A., Czaia, L.,Anderson, D. Z., Zgonik, M., Gunter, P., Phys. Rev. A **52**, 1791 (1995)
[44] Neumann, J., Jakel, G., Kratzig, E., Opt. Lett. **20**, 1530 (1995)
[45] Jakel, G., Neumann, J., Odoulov, S., van Olfen, U., Kratzig, E., Appl. Phys. B **61**, 415 (1995)
[46] Neumann, J., Jakel, G., Kratzig, E., Appl. Phys. B **63**, 599 (1996)
[47] Jakel, G., Neumann, J., Odoulov, S., Kratzig, E., Ferroelectrics **183**, 185 (1996)
[48] Belabaev, K. G., Kiseleva, I. N., Obukhovski, V. V., Odulov, S. G., Taratuta, R. A., Sov. Phys. Solid State **28**, 321 (1986)
[49] Imlau, M., Woike, T., Schieder, B., Rupp, R. A., Phys. Rev. Lett. **82**, 2860 (1999)
[50] Imlau, M., Schieder, R., Rupp, R. A., Woike, T., Appl. Phys. Lett. **75**, 16(1999)
[51] M. A. Ellabban, M. Fally, R. A. Rupp, Th. Woike, M. Imlau, "Holographic scattering and its applications", Recent Research Developments in Applied Physics, **3** (2001) Publisher: Transworld Research Network, India
[52] Amodei, J. J., Appl. Phys. Lett. **18**, 22 (1971)
[53] White, J. O., Cronin-Golomb, M., Fischer, B., Yariv, A., 1982. Appl. Phys. Lett. **40**, 450(1982)
[54] Sturman, B. I., Fridkin, V. M.,The Photovoltaic and Photorefractive Effects in Noncentrosymmetric Materials, Vol. 8 of Ferroelectricity and Related Phenomena (Gordon and Breach Science Publishers, Philadelphia, 1992), Chap. 4, pp. 135-173
[55] Yariv, A., Pepper, D., Opt. Lett. **1**, 16 (1977)
[56] Rupp, R. A., Appl. Phys. A **55**, 2 (1992)
[57] Augustov, P., Reinfelde, M., Shvarts, K., Appl. Phys. A**29**, 169 (1982)
[58] el Guibaly, F., Young, L., Ferroelectrics **46**, 201(1983)
[59] Knyazkov, A. V., Lobanov, M. N., Krumins, A., Seglins, J., Ferroelectrics **69**, 81 (1986)
[60] Marotz, J., Ringhofer, K. H., Rupp, R. A., Treichel, S., IEEE J. Quant. Electron. QE- **22**, 1376 (1986)
[61] Zhang, G., Li, Q.-X., Ho, P.-P., Liu, S., Wu, Z. K., Alfano, R. R., Appl. Opt. **25**, 2955 (1986)
[62] Rupp, R. A., Ringhofer, K. H., Drees, F. W., Marotz, J., Treichel, S., Kratzig, E., in Proceedings of the Sixth IEEE International Symposium on Applications of Ferroelectrics (IEEE, New York, NY, USA, 1986), p. 72.
[63] Feinberg, J., Opt. Lett. **7**, 486 (1982)
[64] M. Goulkov, T. Granzow, U. Dörfler, Th. Woike, M. Imlau, R. Pankrath, Appl. Phys. B. published online (2003)
[65] M. Goulkov, T. Granzow, U. D"orfler, Th. Woike, M. Imlau, R. Pankrath, W. Kleemann, Opt. Commun. **218**, 173 (2003)
[66] M. Goulkov, M. Imlau, R. Pankrath, T. Granzow, U. Dr̈fler, Th. Woike, J. Opt. Soc. Am. B, **20**, 307 (2003)
[67] Ellin, H. C., Solymar, L., Opt. Commun. **130**, 85 (1996)
[68] Marotz, J., Ringhofer, K. H., Rupp, R. A., 31 Technical Digest Series 106 (1987)
[69] M. Goulkov, S. Odoulov, Th. Woike, J. Imbrock, M. Imlau, L. Bäumer, H. Hesse, E. Krätzig, Phys. Rev. B **65**, 195111 (2002)
[70] Odoulov, S. G., Sov. Phys. JETP Lett. **35**, 10 (1982)
[71] Holtmann, L., Kratzig, E., Odoulov, S., Appl. Phys. B **53**, 1 (1991)
[72] . Avakyan, E. M., Alaverdyan, S. A., Belabaev, K. G., Sarkisov, V. K., Tumanyan, K. M., Sov. Phys. Solid State **20**, 1401 (1978)
[73] Sturman, B. I., Odoulov, S. G., Goulkov, M. Y., Phys. Rep. **275**, 197 (1996)
[74] Kukhtarev, N. V., Kratzig, E., Kulich, H. C., Rupp, R. A., Albers, J., Appl. Phys. B **35**, 17 (1984)
[75] Marotz, J., 1985. Appl. Phys. B 37, 181.
[76] Sturman, B. I., Goul'kov, M. Y., Odoulov, S. G., 1996. J. Opt. Soc. Am. B 13, 577.
[77] Odoulov, S., van Olfen, U., Kratzig, E., 1992. Appl. Phys. B 54, 313.
[78] Sun, Q., Liu, Y. S an Zhang, Zhang, G. Q., Fang, Q.,

Tian, G., Xu, J., 1997. Optik 105, 74.
[79] Parshall, E., Cronin-Golomb, M., Barakat, R., 1995. Opt. Lett. 20, 432.
[80] Obukhovski, V. V., Stoyanov, A. V., 1986. Sov. Phys. Solid State 28, 225.
[81] Obukhovski, V. V., Stoyanov, A. V., 1987. Sov. Phys. Solid State 29, 1678.
[82] Lam, J. F., 1985. Appl. Phys. Lett. 46, 909.
[83] Sturman, B. I., 1991. Sov. Phys. JETP 73, 593.
[84] Stepanov, S. I., Petrov, M. P., 1985. Opt. Commun. 53, 292.
[85] Zhao, F., Zhou, H., Wu, Z., Yu, F. T. S., McMillen, D. K., 1996. Opt. Engineering 35, 1985.
[86] He, B. Q., Yeh, P., 1994. Appl. Opt. 33, 283.
[87] Rupp, R. A., Kerperin, K., Krumins, A., 1989. Ferroelectrics 90, 75.
[88] Rupp, R. A., Sommerfeldt, R., Ringhofer, K. H., Kratzig, E., 1990. Appl. Phys. B 51, 364.
[89] Clark III, W. W., Wood, G. L., Miller, M. J., Sharp, E. J., Salamo, G. J., Monson, B., Neurgaonkar, R. R., 1990. Appl. Opt. 29, 1249.
[90] Kostuk, R. K., Sincerbox, G. T., 1988. Appl. Opt. 27, 2993.
[91] Belendez, A., Carretero, L., Pascual, I., 1993. Appl. Opt. 32, 7155.
[92] Belendez, A., Fuentes, R., Fimia, A., 1993. J. Optics (Paris) 24, 99.
[93] Voronov, V. V., Dorosh, I. R., Kuz'minov, Y. S., Tkachenko, N. V., Sov. J. Quantum Electron. **10**, 1346 (1980)
[94] Ducharme, S., Feinberg, J., Neurgaonkar, R. R., 1987. IEEE J. Quant. Electron. QE- 23, 2116.
[95] Dorfler, U. B., Piechatzek, R., Woike, T., Imlau, M. K., Wirth, V., Bohaty, L., Volk, T., Pankrath, R., Wohlecke, M., 1999. Appl. Phys. B 68, 843.
[96] Buse, K., Van Stevendahl, U., Pankrath, R., Kratzig, E., 1996. J. Opt. Soc. Am. B 13, 1461.
[97] Buse, K., 1997. Appl. Phys. B 64, 273.
[98] Vazquez, R. A., Vachss, F. R., Neurgaonkar, M. D. R. R. Ewbank, J. Opt. Soc. Am. B **8**, 1932 (1991)
[99] Rupp, R. A., Seglins, J., van Olfen, U., 1991. Phys. Stat. Sol. (b) 168, 445.
[100] Abrahams, S. C., Jamison, P. B., Bernstein, J. L., 1971. J. Chem. Phys. 54, 2355.
[101] Lehnen, P., Kleemann, W., Woike, T., Pankrath, R., 2000. Eur. Phys. J. B 14, 633.
[102] T. Granzow, Th. Woike, W. Rammensee, M. Woehlecke, M. Imlau, R. Pankrath, Phys. Stat. Sol. (a), **197**, R2-R4 (2003)
[103] Woike, T.,Weckwerth, G., Palme, H., Pankrath, R., 1997. Solid State Commun. 102, 743.
[104] Wingbermuhle, J., Meyer, M., Schirmer, O. F., Pankrath, R., Kremer, R. K., 2000. J. Phys.: Condens. Matter 12, 4277.
[105] Dec, J., Kleemann, T. W. Woike, Pankrath, R., 2000. Eur. Phys. J. B 14, 627.
[106] Lehnen, P., Dec, J., Kleemann, T. W. Woike, Pankrath, R., 2000. Ferroelectrics 240, 281.
[107] M. D. Ewbank, R. R. Neurgaonkar, W. K. Cory, and J. Feinberg, J. Appl. Phys. **62**, 374 (1987)
[108] N. V. Kukhtarev, V. P. Markov, S. G. Odoulov, M. S. Soskin, V. L. Vinetskii, Ferroelectr. **22**, 961 (1979)
[109] P. Yeh, Introduction to photorefractive nonlinear optics, John Wiley, New York (1993)
[110] U. B. Dörfler, R. Piechatzeck, Th. Woike, M. Imlau, v. Wirth, L. Bohaty, T. volk, R. Pankrath, M. Wöhlecke, Appl. Phys. B **68**, 843 (1999)
[111] J. R. Oliver, r. R. Neurgaonkar, L. E. cross, J. Appl. Phys. **44**, 254 (1973)
[112] T. Granzow, U. Dörfler, Th. Woike, M. Wöhlecke, R. Pankrath, M. Imlau, W. Kleemann, Phys. Rev. B **63**, 174101 (2001)
[113] Th. Woike, T. Granzow, U. Dörfler, Ch. Pötsch, M. Wöhlecke, R. Pankrath, Phys. Stat. Sol. (a) **186**, R13 (2001)
[114] J. Dec, W. Kleemann, Th. Woike and R. Pankrath, Eur. Phys. J. B **14**, 627 (2000)
[115] L. E. Cross, Ferroelectrics **76**, 241 (1987)
[116] A. S. Bhalla, R. Guo, L. E. Cross, G. burns, F. H. Dacol, R. R. Neurgaonkar, Phys. Rev. B **36**, 2030 (1987)
[117] V. Wirth, Temperaturabhängige elektrooptische und elektrostriktive Untersuchungen an Kristallen mit ferroischen Phasenumwandlungen, Dissertation Köln (1999)
[118] A. J. Fox, J. Appl. Phys. **44**, 254 (1973)